18TH WORLD CONFERENCE ON EARTHQUAKE ENGINEERING
WCEE2024
MILAN

MILAN, ITALY
30TH JUNE - 5TH JULY 2024
www.wcee2024.it

ELASTIC LOCAL BUCKLING STRESS OF LIPPED CHANNEL MEMBERS SUBJECTED TO ECCENTRIC COMPRESSION

T. Kobashi[1], K. Mitsui[2], R. Kuwada[3] & K. Ikarashi[4]

[1] Chiba Institute of Technology, Chiba, Japan, kobashi.tomoki@p.chibakoudai.jp

[2] Tokyo Institute of Technology, Tokyo, Japan

[3] Nippon Steel Corporation, Chiba, Japan

[4] Tokyo Institute of Technology, Tokyo, Japan

Abstract: *Cold-formed steel members that are framed inside the wall panel transmit the horizontal force caused by earthquakes to the foundation as an axial force. Therefore, they should have enough axial loading capacity to prevent the collapse of the wall panel. These members are restrained from global buckling by surrounding structural components. Consequently, their loading capacity is affected by their local buckling strength. When we evaluate the loading capacity of the axially compressed members, we generally assume that the compression force is loaded at the centroidal axis. However, in the case of practical structures, the axial force is loaded from the sheet element and/or specific connectors so that the load acting point is decentered. Furthermore, the local buckling strength of the cold-formed steel members is usually evaluated by regarding the plate elements that consist of the member cross-section as simply supported plates. However, all plate elements have another adjacent plate, and the rotation of the longitudinal edge is restrained. Therefore, in this paper, the elastic local buckling stress of eccentrically compressed lipped channels is investigated. Eigenvalue analyses by the finite strip method were conducted, and design equations for the elastic local buckling stress of the web, flange, and lip are proposed. The proposed design equations can consider the restraining effect that caused by adjacent plate element. By comparing the results from the numerical analysis and the proposed design method, we found that the local buckling load obtained from eigenvalue analyses corresponds well with the evaluation results obtained from the proposed design formulas.*

1. Introduction

Cold-formed steel is used as the primary structural component in low-rise and mid-rise buildings in Japan, ranging from 1-story to 4-story (Fujihashi et al. (2023)). These buildings have wall panels designed to resist lateral forces caused by earthquakes. In the case of wall-panel structures, the lateral shear force from earthquakes is transmitted to the foundation through the stud members framed inside the wall panels (see Figure 1). Therefore, the stud members should possess sufficient strength to prevent the collapse of the wall panels.

The stud is constrained by its surrounding structural components, limiting its global buckling. Therefore, the loading capacity of the stud is defined by local buckling. The stud member usually has a lipped channel cross section, thus many investigations about the local buckling load of axially compressed lipped channels have been conducted. Based on the results of these previous researches, the current American Iron and Steel

Institute (AISI) design specifications (AISI (2016)) provide design formulas for the local buckling load of the web, flange, and lip.

These current design formulas assumed that the plate element of which the cross-section is composed behaved as a simply supported plate element. On the other hand, in the case of the practical member, all plate elements have an adjacent plate element, therefore the rotation of the longitudinal edge is restrained; this restraining effect induces an increase in the local buckling load of the plate element.

In recent years, some investigations that focused on the restraining effect between adjacent plate elements were also conducted. Kobashi et al. conducted studies on the local buckling behavior of rectangular sections under compression (Kobashi et al. (2018)) and bending (Kobashi et al. (2019)). They proposed design formulas for the elastic local buckling stress that can consider the restraining effect between adjacent plate elements. Mitsui et al. (Mitsui et al. (2021) and Mitsui et al. (2023)) developed a design formula for axially compressed lipped channel members based on the energy method by approximating the buckling mode of the lipped channels. Kobashi et al. (Kobashi et al. (2023)) developed a design formula for the lips under compression, considering the restraining effect from the flange.

When we focus on the stud framed inside the wall panel, the axial force is applied to the stud through the sheet element and/or specific connectors, so the axial forces do not act on the centroidal axis of the lipped channel cross section. However, there is no existing design method to evaluate the elastic local buckling stress when the loading point is decentered. Therefore, we need to conduct experiments or complicated numerical analyses when we determine the loading capacity of the stud members subjected to eccentric compression.

The objective of this research is to investigate the elastic local buckling stress of cold-formed steel members under eccentric axial compression. In this paper, we focused on the buckling behavior of lipped channel members and worked on developing a design formula to evaluate the elastic local buckling stress of the web, flange, and lip. Furthermore, we conducted eigenvalue analysis using the finite strip method and compared the analysis results with the proposed design equation results.

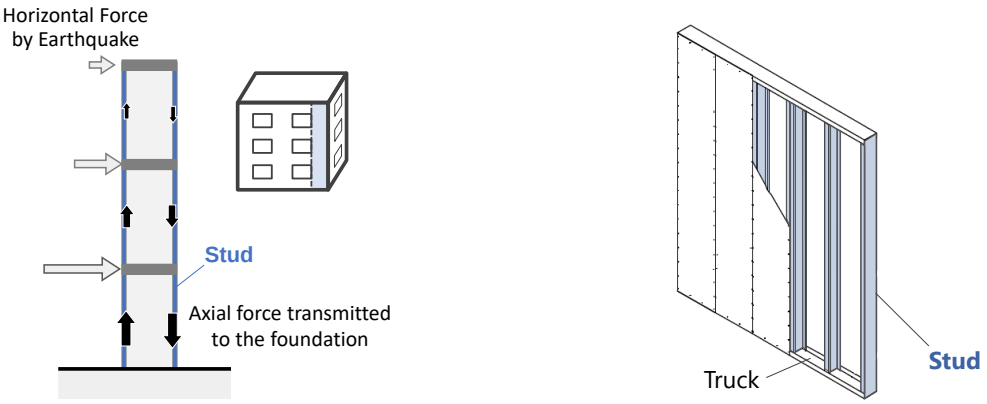

(a) Axial force loaded on the stud by an earthquake *(b) Overview of the wall-panel*

Figure 1. Axial compression force on the stud members framed inside a wall panel

2. Buckling coefficient of the flange, web, and lip

It is well known that the elastic local buckling stress of the plate element can be evaluated using the following equation.

$$\sigma_{cr} = k\frac{E\pi^2}{12(1-\nu^2)}\left(\frac{t}{b}\right)^2 \quad (1)$$

Where k : Buckling coefficient of the plate element [-]
E : Young's modulus [N/mm^2]
ν : Poison's ratio [-]
t : Thickness of the plate element [mm]
b : Width of the plate elements [mm]

The buckling coefficient *k* is a value that determined by the stress distribution and the boundary conditions at the plate edges. For example, the AISI specifications provided design formulas about the buckling coefficient k_p as follows. Note that the following equations are rewrite f_1 / f_2 into 1-ξ . The f_1 and f_2 are existing stress at the plate edges as shown in Figure 2, where $|f_2| \geqq |f_1|$.

a) Web and Flange

$$k_p = 4 + 2(\xi^3 + \xi) \tag{2}$$

b) Lip

[In the case supported edge is in compression side]

For $0 \leq \xi < 1$

$$k_p = \frac{0.578}{1.34 - \xi} \tag{3.1}$$

For $1 \leq \xi < 2$

$$k_p = 13.8 - 29.2\xi + 17.1\xi^2 \tag{3.2}$$

[In the case free edge is in compression side]

$$k_p = 0.43 + 0.07\xi + 0.07\xi^2 \tag{4}$$

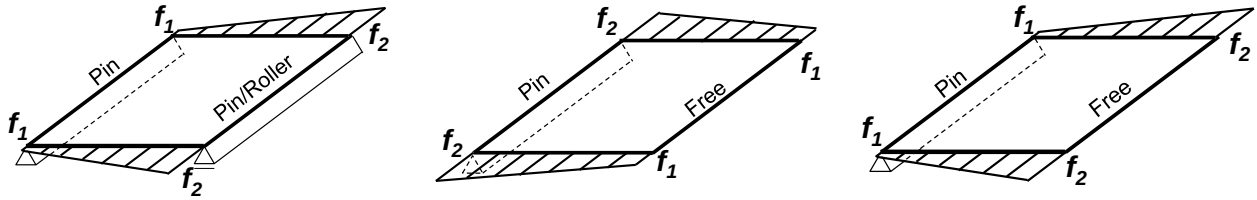

(a) Flange and web (simply supported plate) *(b) Lip (Stress at pinned edge equals f_2)* *(c) Lip (Stress at free edge equals f_2)*

Figure 2. Stress distribution and boundary conditions that AISI specifications can be applied

These design formulas could be considered an effect of the stress gradient. However, they assumed simply supported conditions or free longitudinal edge, so that they did not consider the restraining effect between adjacent plate elements. Thus, in this section, we work on developing the design formula for the buckling coefficient of flange, web, and lip with considering the restraining effect between adjacent plate elements.

2.1. Buckling coefficient of the web

In the case of web, both longitudinal edges are restrained in their rotation by flanges. The design formula for the buckling coefficient of the web under axial compression and bending moment had been presented in Kobashi (2019) as follows.

$$k = \gamma k_p + (1 - \gamma) k_r \tag{5}$$

k_p represent a buckling coefficient of a simply supported plate obtained from Eq.(2), and k_r represents a buckling coefficient of a rigidly restrained plate obtained from the following equation (Kobashi (2019)).

$$k_r = 6.98 + 3.26(\xi^3 + \xi) \tag{6}$$

γ in Eq.(6) is a dimensionless quantity that changes from zero to unity. Thus, Eq.(5) suggests that the magnitude of *k* is between k_p and k_r. Furthermore, design formulas for γ are also presented in Kobashi (2019) as follows.

$$\text{For } 0 < \frac{b_{ad}}{b_b}\sqrt{\frac{k_{p\_b}}{k_{p\_ad}}} \leq 0.1 \qquad \gamma = 4.6\frac{b_{ad}}{b_b}\sqrt{\frac{k_{p\_b}}{k_{p\_ad}}} \tag{7.1}$$

$$\text{For } 0.1 < \frac{b_{ad}}{b_b}\sqrt{\frac{k_{p\_b}}{k_{p\_ad}}} \leq 1.0 \qquad \gamma = 0.4 + 0.6\frac{b_{ad}}{b_b}\sqrt{\frac{k_{p\_b}}{k_{p\_ad}}} \tag{7.2}$$

$$\text{For } \ 1.0 < \frac{b_{ad}}{b_b}\sqrt{\frac{k_{p\_b}}{k_{p\_ad}}} \qquad \gamma = 1 \qquad (7.3)$$

b_b and k_{p_b} represent the plate width and the buckling coefficient of a buckled plate, respectively. Furthermore, b_{ad} and k_{p_ad} represent the plate width and the buckling coefficient of an adjacent plate element, respectively. It is assumed that both k_{p_b} and k_{p_ad} are the buckling coefficients of a simply supported plate. Although these equations do not assume that the lipped channel is subjected to bending moment around the miner axis, we can obtain values for b_b, b_{ad}, k_{p_b}, and k_{p_ad} from the cross-section shapes and Eq.(2). Therefore, in this paper, we employ these design formulas to evaluate the buckling coefficient of the web.

2.2. Buckling coefficient of the flange

In the case of the flange, one longitudinal edge is connected to the web, and the other longitudinal edge is connected to the lip, thus the boundary conditions for these two edges are different. When we focus on the restraining effect between adjacent plate elements, the rotational restraint is caused by the bending stiffness of the adjacent plate element. However, in the case of the lip, one longitudinal edge is connected to the flange and the other longitudinal edge is unstiffened, so the lip is assumed to not have enough stiffness to restrain the rotation of flange's longitudinal edge. Therefore, it was assumed that the flange is restrained the rotation of the longitudinal edges only by the web; and ignore the restraint from the lip to the flange.

In this paper, the buckling coefficient k is evaluated using Eq. (5). In the case of the flange, the longitudinal edges are supported by the web and lip, allowing k_p to be evaluated as a simply supported plate element (Eq.(2)). Furthermore, as shown in Figure 3, k_r can be obtained by assuming that the plate is in a boundary condition where one longitudinal edge (Edge-A in Figure 3) is simply supported, and the other longitudinal edge (Edge-B in Figure 3) is rigidly restrained.

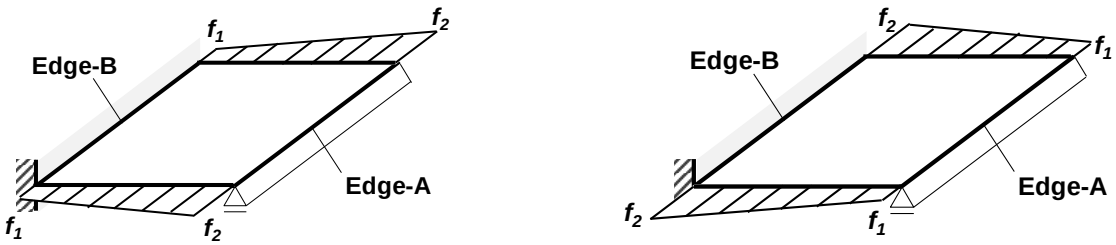

(a) In the case that stress at Edge-A equals f_2 *(b) In the case that stress at Edge-B equals f_2*

Figure 3. Plate element with one longitudinal edge is restrained its rotation

In the case where only axial compression force is applied to the plate (i.e., $f_1 = f_2$), the buckling coefficient is equal to 5.41. Furthermore, in the case where in-plane bending is applied, if Edge-A is compressed by bending moment, the buckling coefficient is equal to 24.48. Additionally, when Edge-B is compressed by bending moment, even though the tensile edge is pinned, the buckling coefficient is considered to be approximately equal to that of a plate with both longitudinal edges restrained (equal to 39.6). Therefore, in this study, the buckling coefficient of a plate subjected to both bending moment and axial compressive force is evaluated as follows, referring to Eq. (2) and Eq. (6). Eq. (8.1) assumes that Edge-A is on the compression side, as shown in Figure 3(a), and Eq. (8.2) assumes that Edge-B is on the compression side, as shown in Figure 3(b). Note that $\xi = 1 - f_1/f_2$ in the equation.

$$k_r = 5.41 + 1.91(\xi^3 + \xi) \qquad (8.1)$$

$$k_r = 5.41 + 3.42(\xi^3 + \xi) \qquad (8.2)$$

Eigenvalue analyses were conducted to investigate the accuracy of Eq. (8.1) and (8.2) using the finite strip analysis program CU-FSM (Li et al., 2010). The analysis model is a plate element, as shown in Figure 3. In this model, the compression side or tensile side is rigidly restrained in rotation. We assumed that the plate consists of steel material with a Young's modulus of E = 205,000 N/mm² and a Poisson's ratio of v = 0.3. The plate width is 100 mm, and the plate thickness is 1.0 mm.

Figure 4 shows the analysis results. The vertical axis represents the buckling coefficient back calculated from the analysis results using Eq. (1). Broken lines represent the results of the proposed equations (Eq. (8.1) and (8.2)). Black and white plots represent the eigenvalue analysis results. Black plots represent the analyses where Edge-A is compressed, and white plots represent those where Edge-B is compressed. It was found that the proposed design formula corresponded well with the numerical analysis results.

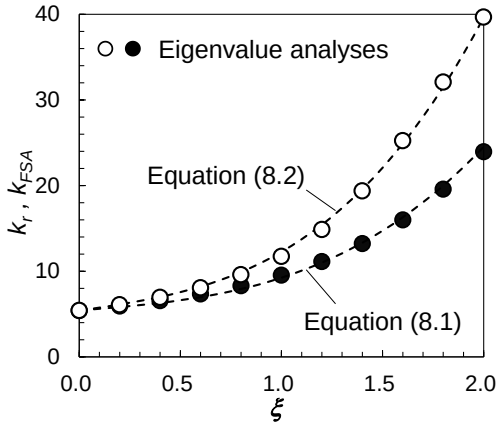

Figure 4. Comparison of eigenvalue analyses and proposed equation results

2.3. Buckling coefficient of the lip

In the case of the lip, one longitudinal edge is free, so the restraining occurs only from the adjacent flange. By focusing on this boundary condition, Kobashi et al. (2023) have developed the design formula for the lip under compression as follows.

$$k = k_p + \sqrt{1-\gamma}\left(k_r - k_p\right) \tag{9}$$

In this paper, we assumed that Eq. (9) can be applied to the lip when it is loaded under axial compression and bending moment simultaneously. According to the AISI specifications, k_p can be obtained from Eq. (3.1), (3.2), and (4). These equations assume that one longitudinal edge is in a simply supported condition. Therefore, we conducted an eigenvalue analysis of the plate with one longitudinal edge rigidly restrained, as shown in Figure 5, and worked on approximating the relationship between k_r and ξ. Figure 5 provides an overview of the analysis models. Figure 5(a) represents a model where stress decreases towards the free edge, while Figure 5(b) represents a model where stress increases towards the free edge. The plate is made of steel material with a Young's modulus of E = 205,000 N/mm² and a Poisson's ratio of ν = 0.3. The plate has a width of 100 mm and a thickness of 1.0 mm.

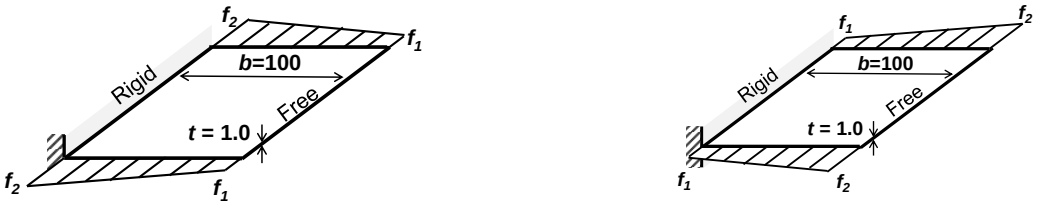

(a) In the case that stress at rigid edge equals f_2 *(b) In the case that stress at free edge equals f_2*

Figure 5. Analysis model of unstiffened element

Figure 6 shows the analysis results. The vertical axis represents the buckling coefficient, and the horizontal axis represents ξ. The black and white plots represent the analysis results, of which the buckling coefficient were derived from a back-calculation of the analysis results. The broken lines represent the approximation results based on Equations (10.1), (10.2), and (11). These equations were obtained by approximating the constant coefficients in Equations (3.1), (3.2), and (4), respectively. From Figure 6, it can be observed that the k_r obtained from the proposed corresponded well with the numerical analysis results.

[In the case supported edge is in compression side]

For $0 < \xi \leq 1$

$$k_r = \frac{1.62}{1.27 - \xi} \quad (10.1)$$

For $1 < \xi \leq 2$

$$k_r = -22.7 + 26.3\xi + 2.37\xi^2 \quad (10.2)$$

[In the case free edge s compression side]

$$k_r = 1.28 + +0.22\xi + 0.10\xi^2 \quad (11)$$

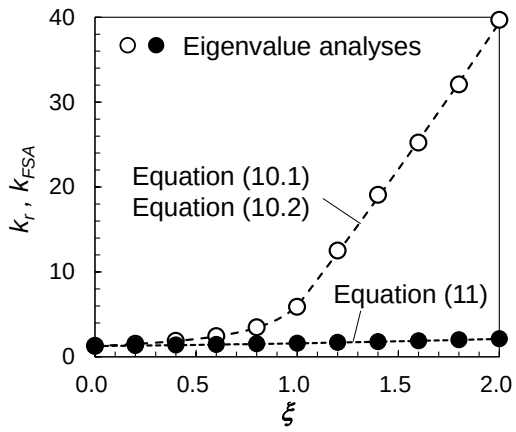

Figure 6. Comparison of eigenvalue analyses and proposed equation results

3. Eigenvalue analyses by the Finite Strip Method

3.1. Summary of Analysis

To examine the elastic local buckling stress of lipped channel members, we conducted Finite Strip Analysis (FSA) using CUFSM. Figure 7 shows a cross-section of the analysis model. In this analysis, we investigated the elastic local buckling load of lipped channel members subjected to eccentric compression forces. Table 1 shows the analysis variables. In this study, we varied the web depth (b_w), plate thickness (t), eccentric distance (e), and angle (θ). The lipped channel is made of steel material with a Young's modulus of E = 205,000 N/mm² and a Poisson's ratio of ν = 0.3. To prevent unexpected distortional buckling, the displacement in the z-direction at the corner between the lip and the flange is fixed.

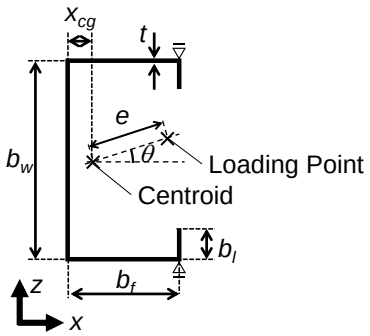

Figure 7. Cross-section of the analysis model

Table 1. Analysis variables

b_w [mm]	b_f [mm]	b_l [mm]	t [mm]	e/x_{cg} [-]	θ [rad]
100, 150	40	12	1, 1.6, 2.2	0.0 – 5.0 @ 0.5	0.0 - π @ π/8

In this paper, we assumed that the stress distribution at the cross-section can be approximated as a combined action of compression and bending. Based on this assumption, the stress on the cross section can be obtained

as follows from the Bernoulli-Euler theory. Here, A represents the gross cross-section of the lipped channel, Z_x is the section modulus around the *x*-axis, and Z_z is the section modulus around the *z*-axis. The terms f_a, f_{bx}, and f_{bz} represent the stresses caused by axial compression forces or bending moments around the major axis and minor axis, respectively.

$$f = f_a + f_{bs} + f_{bw\_i} \tag{12.1}$$

$$f_a = \frac{N}{A} \tag{12.2}$$

$$f_{bx} = \frac{Ne \sin\theta}{Z_x} \tag{12.3}$$

$$f_{bz} = \frac{Ne \cos\theta}{Z_z} \tag{12.4}$$

3.2. Analysis results and Considerations

3.2.1. Effect of eccentricity

Figure 8 shows the analysis results. The horizontal axis represents the length *e*, and the vertical axis represents σ_{cr}/σ_{ccr}, where σ_{cr} represents the elastic local buckling stress obtained through numerical analysis, and σ_{ccr} represents the elastic local buckling stress in cases where axial compression force is loaded on a centroidal axis. From the figures, it was found that the difference in plate thickness *t* does not have a significant effect on the analysis results.

Furthermore, in the cases where θ equals 0 and $\pi/4$, σ_{cr}/σ_{ccr} increased as e decreased. Then, σ_{cr}/σ_{ccr} reached its maximum value and gradually decreased with an increase in *e*. On the other hand, in the cases where θ equals $\pi/2$, $3\pi/4$, and π, σ_{cr}/σ_{ccr} gradually decreased with an increase in *e*.

In the case of lipped channel members subjected to eccentric compression forces, when the loading point shifts from the centroidal axis towards the lip direction, the existing stress on the web decreases, while that on the lip and flange increases. Due to this stress gradient, the occurrence of elastic local buckling in the web is restrained, the buckling load of the lipped channels were increased, as shown in Figure 8(a) and (b).

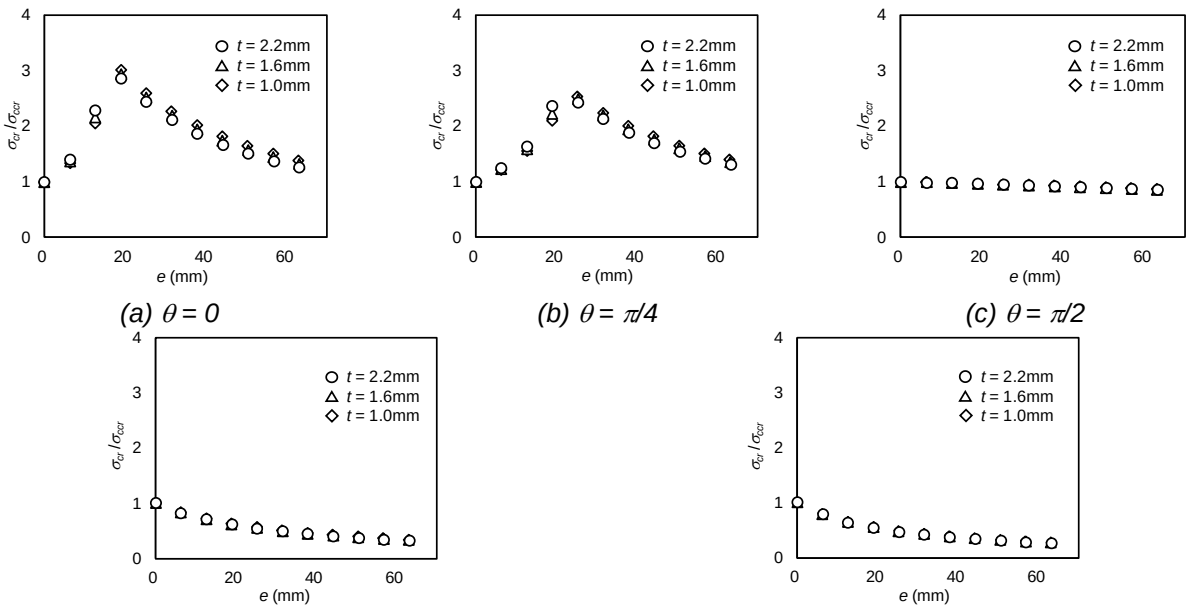

(a) $\theta = 0$ (b) $\theta = \pi/4$ (c) $\theta = \pi/2$

(d) $\theta = 3\pi/4$ (e) $\theta = \pi$

Figure 8. Elastic local buckling stress of the lipped channels under eccentric compression

3.2.2. Evaluation results by the proposed method

Figures 9 and 10 present evaluation results for elastic local buckling stress using the proposed design formulas as mentioned in Section 2. Figure 9 represents the numerical analysis results for b_w = 100mm and t = 1.6mm, while Figure 10 represents the same for b_w = 150mm and t = 1.6mm. The parameter e takes values of e = 0.5x_g, 1.0x_g, 2.0x_g, and 5.0x_g. The horizontal axis represents the angle θ, and the vertical axis represents $\sigma_{FSA}/\sigma_{cr\_r}$, where σ_{FSA} represents the maximum stress on the plate when the member reaches its elastic local buckling load and is obtained from eigenvalue analysis results. Furthermore, σ_{cr_r} represents the elastic local buckling stress obtained from the proposed design method. White plots represent results for the web, black plots represent results for the flange, and gray plots represent results for the lip.

In the case of e=0.5x_g and 1.0x_g, $\sigma_{FSA}/\sigma_{cr\_r}$ for the web is greater than that for the flange and lip. These results suggest that the elastic local buckling stress of the web is lower than that of the flange and lip, indicating that local buckling of the lipped channel primarily occurs at the web. When the loading point is displaced toward the lip direction, a bending moment that induces tension on the web and compression on the lip increases due to eccentricity. This bending moment reduces the compressive stress on the web while increasing the compressive stress on the lip. Consequently, the existing stress on the lip and flange increases when the existing stress on the web reaches its elastic local buckling stress. Therefore, $\sigma_{FSA}/\sigma_{cr\_r}$ for the flange and lip also increases with an increase in e.

In the cases of e = 2.0x_g and 5.0x_g, as e increases, it was observed that $\sigma_{FSA}/\sigma_{cr\_r}$ for the web falls below 1.0, while that for the flange and the lip approaches unity within the range of θ smaller than π/2. Due to the eccentricity of the loading point, the existing stress on the web transitions from compression to tension, and the possibility of web buckling disappears. Consequently, in the range where θ is small, local buckling occurs at the flange and lip, and $\sigma_{FSA}/\sigma_{cr\_r}$ for the flange and lip approaches unity.

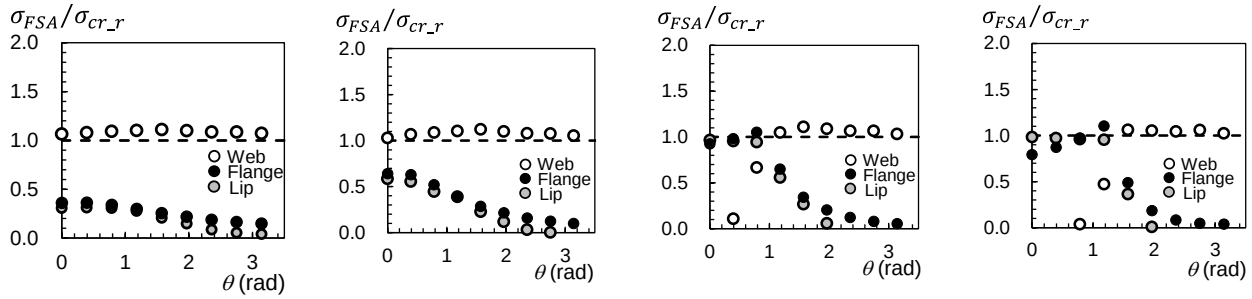

(a) e=0.5x_g *(b) e=1.0x_g* *(c) e=2.0x_g* *(d) e=5.0x_g*

Figure 9. Evaluation results of elastic local buckling stress about the web, flange, and lip (b_w = 100mm and t = 1.6mm)

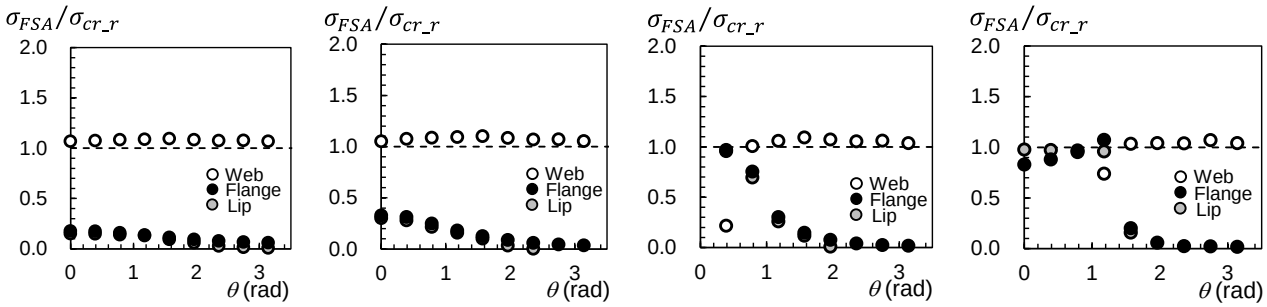

(a) e=0.5x_g *(b) e=1.0x_g* *(c) e=2.0x_g* *(d) e=5.0x_g*

Figure 10. Evaluation results of elastic local buckling stress about the web, flange, and lip (b_w = 150mm and t = 1.6mm)

Assuming that the elastic local buckling of the lipped channel is induced when the existing stress on each plate element reaches the plate elastic local buckling stress, we evaluate the elastic local buckling stress of lipped channels subjected to eccentric compression. In this paper, we assess the ratio of eigenvalue analysis results to the results obtained from the proposed design equations as follows. Where f_{fw} represents the existing stress between the flange and web, f_{fl} represents the existing stress between the flange and lip. σ_{cr_f}, σ_{cr_w}, and σ_{cr_l} represent the calculated elastic local buckling stress of the flange, web, and lip, respectively.

For $\theta < \pi/2$

$$\frac{\sigma_{FSA}}{\sigma_{cr\_cal}} = \max\left(\frac{f_{fw}}{\sigma_{cr\_w}} \quad \frac{f_{fl}}{\sigma_{cr\_f}} \quad \frac{f_{fl}}{\sigma_{cr\_l}}\right) \tag{13.1}$$

For $\theta \geq \pi/2$

$$\frac{\sigma_{FSA}}{\sigma_{cr\_cal}} = \max\left(\frac{f_{fw}}{\sigma_{cr\_w}} \quad \frac{f_{fw}}{\sigma_{cr\_f}} \quad \frac{f_{fl}}{\sigma_{cr\_l}}\right) \tag{13.2}$$

Figure 11 displays the evaluation results for the elastic local buckling load subjected to eccentric compression forces. The vertical axis represents $\sigma_{FSA}/\sigma_{cr\_cal}$, and the horizontal axis represents θ. The white plots represent the numerical analysis results, and the dashed line represents where $\sigma_{FSA}/\sigma_{cr\_cal}$ equals 0.9 or 1.1. The Mean and C.V. in the figure represent the average and coefficient of validity of $\sigma_{FSA}/\sigma_{cr\_cal}$, respectively. It was observed that the plots are existed around $\sigma_{FSA}/\sigma_{cr\_cal}$ = 1.0. Furthermore, the average value is close to unity, and the coefficient of validity is 4%. Based on these findings, we conclude that the proposed design formula can effectively evaluate the elastic local buckling load of lipped channel members subjected to eccentric compression forces with an error of around 10% or less.

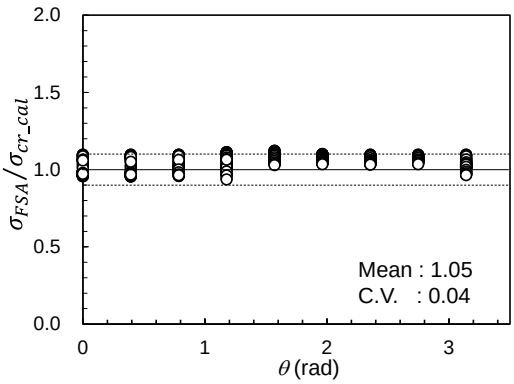

Figure 11. Evaluation results by the proposed method

4. Conclusions

This paper investigated the elastic local buckling load of lipped-channel members subjected to eccentric compression forces. Design formulas for the elastic local buckling stress of the flange, web, and lip were proposed, considering the restraining effect between adjacent plate elements. We compared the evaluation results with the elastic local buckling stress obtained through eigenvalue analysis.

In the case of lipped channel members subjected to eccentric compression forces, when the loading point shifts from the centroidal axis towards the lip direction, the existing stress on the web decreases, while that on the lip and flange increases. This stress gradient leads to an increase in the elastic local buckling load of the lipped channel.

Furthermore, through the comparison between the numerical analysis results and the evaluation results obtained using the proposed method, we concluded that the elastic local buckling load of the lipped channel can be assessed by using the local buckling stress of the plate elements that constitute the member's cross section. Clarifying the cross-section shapes that applicable to the proposed method is a future research issue.

5. References

Fujihashi K., Tohnai S., Katsuo M., Sato K., Kobashi T., Oonari K., Nakamura D., Kawai Y.(2023). Diversification of building sheet products/structural properties and energy saving performance of light-gauge steel framed houses, *NIPPON SEITETSU GIHOU*, vol.420, pp.98-103 (In Japanese)

AISI (2016). *North American Specification for the Design of Cold-Formed Steel Structural Members-AISI S100-16*, American Iron and Steel Institute, Washington D.C.

Kobashi T., Ikarashi K., Shimizu N. (2018). Elastic local buckling strength and maximum strength of cold formed steel members with different plate width on adjacent plate elements, *Journal of Structural and Construction Engineering (Transactions of AIJ)*, 83(749), 1051-1061 (In Japanese)

Kobashi T., Ikarashi K., Shimizu N. (2019). Elastic local buckling strength and maximum strength of rectangular section members which were loaded compression and bending, *Journal of Structural and Construction Engineering (Transactions of AIJ)*, 84(755), 97-107 (In Japanese)

Kobashi T. (2019). Design equations for elastic local buckling strength of lipped-C channel members, *Proceedings of the 12th pacific structural steel conference*, Tokyo, Japan

Mitsui K., Ikarashi. K. (2021). Buckling strength and behavior of elastic local buckling for cold-formed channel member under compression, *Journal of Structural and Construction Engineering (Transactions of AIJ)*, 86(790), 1685-1692 (In Japanese)

Mitsui K., Ikarashi K., Tomoki K., Ryohei K. (2023). Elastic critical local buckling stress in cold-formed lipped channel and hat sections under uniform compression, *Thin-Walled Structures*, 191

Kobashi T., Mitsui K., Kuwada R., Ikarashi K. (2023). Elastic local buckling load of lip element of cold-formed steel member under compression, *Proceedings of 13th Pacific Structural Steel Conference*, Chengdu, China

Li Z., Schafer B.W. (2010). Buckling analysis of cold-formed steel members with general boundary conditions using CUFSM: conventional and constrained finite strip methods, *Proceedings of the 20th International Speciality Conference on Cold-Formed Steel Structures*, Missouri, USA